Are the interglacial epochs analogue of the Asian-African monsoon response to global warming?

Yuhao Wang (yhwangnuist@163.com)
Ningbo Meteorological Bureau
Chao He
Jinan University
Tim Li
University of Hawaii at Manoa
Chengming Zhang
Ningbo Meteorological Bureau
Xiaoli Gu
Ningbo Meteorological Bureau

Research Article

Keywords: Asian-African monsoon, global warming, interglacial epoch, land-ocean θe contrast, SST warming, atmospheric static stability

Posted Date: February 8th, 2023

DOI: https://doi.org/10.21203/rs.3.rs-2552233/v1

Additional Declarations: No competing interests reported.

Version of Record: A version of this preprint was published at Climate Dynamics on November 30th, 2023. See the published version at https://doi.org/10.1007/s00382-023-07013-0.

Abstract

Precipitation was claimed to increase over Asian and North African monsoon (AAM) regions during past interglacial epochs and also under future global warming scenarios. Using CMIP6 model experiments, this study compares the changes of AAM in interglacial epochs to global warming. Moisture budget analysis shows that the increased monsoon rainfall during interglacial epochs primarily results from the dynamic process associated with strengthened monsoon circulation, but is caused by thermodynamic process under global warming associated with increased mean moisture. To disentangle the mechanism for the distinct changes in vertical and horizontal monsoon circulation, we further decompose the response of AAM to global warming into the direct effect from CO_2 radiative forcing and the indirect effect due to increased sea surface temperature (SST), based on idealized CMIP6 experiments. The results show that the effect of direct CO_2 radiative forcing on the AAM is an analogue to that in interglacial epochs driven by enhanced land-ocean equivalent potential temperature contrast, both of which are characterized by strengthened vertical and horizontal monsoon circulation despite regional difference. However, the above effect is overwhelmed by the substantially increased SST under global warming, which is absent during interglacial epochs. The substantial SST warming acts to weaken the monsoon circulation by decreasing the land-ocean equivalent potential temperature contrast and enhancing the atmospheric static stability. Our results demonstrate that the interglacial epoch is not an analogue of the AAM response to global warming, and the lack of global SST warming is responsible for their difference.

1 Introduction

The Asian-African monsoon (AAM), including the East Asian monsoon (EAM), South Asian monsoon (SAM) and North African monsoon (NAFM), is a crucial system to the hydroclimate in the Northern Hemisphere. The large-scale monsoon circulation brings abundant moisture from the warm tropical ocean to the land monsoon region during boreal summer, and supplies more than half of the annual rainfall (Wang and LinHo 2002). The variability of the AAM is largely modulated by the internal variability of the climate system (Zhang and Delworth 2006; Zhou et al. 2008; Kucharski et al. 2009; Liu et al. 2014; Li et al. 2017b; Wang et al. 2019) or the external forcing (Giannini 2010; Jiang et al. 2015; Li et al. 2015; Shi and Yan 2019; Zuo et al. 2019) and greatly impacts the development of the agriculture and economy (Webster et al. 1998; Gadgil and Rupa Kumar 2006; Mall et al. 2006), which is closely associated with the livelihoods of billions people in the region. It was suggested that the AAM has suffered decadal changes in the observational period (Li et al. 2017b).

Given the profound impact of the ongoing global warming on the climate system, future change of the AAM has received much attention. Forced by the increased concentration of the greenhouse gases, a stronger warming of the Northern Hemisphere relative to the South Hemisphere accompanied with a warmer land than the ocean is projected (Sutton et al. 2007; IPCC 2013; Jones et al. 2013; Wang et al. 2021), and the Northern Hemisphere land monsoon system is generally strengthened (Lee and Wang 2014; Cao et al. 2020; He et al. 2020; Wang et al. 2020a; Wang et al. 2021). For the regional changes, the

Asian summer monsoon rainfall is projected to be robustly increased (IPCC 2013), explained by the “wet-get-wetter” (Held and Soden 2006; Chou et al. 2009) or the “richest-get-richer” (Hsu and Li 2012) mechanism due to the increase of mean moisture. The EAM low-level circulation is suggested to be strengthened (Ueda et al. 2006; Sun and Ding 2010; He and Zhou 2020; Jin et al. 2020), modulated by the enhanced Asian Continent-North Pacific thermal contrast (Sun and Ding 2010; Kamae et al. 2014; Li et al. 2019) associated with the intensified Tibetan Plateau (TP) thermal forcing (He et al. 2019; Li et al. 2022). While the SAM low-level circulation is projected to be weakened (Ueda et al. 2006; Sun et al. 2010; Turner and Annamalai 2012; Menon et al. 2013; Sharmila et al. 2015; Jin et al. 2020; Li et al. 2021). This weakening is argued to result from the decreased tropospheric meridional temperature gradient (Sun et al. 2010; Sooraj et al. 2015; Li et al. 2021). While a recent study attributed this change to the SST warming pattern over the equatorial Pacific (Li et al. 2022). Compared to the Asian summer monsoon, the projection of NAFM rainfall suffers more uncertainty, due to the competition of the effect of the direct radiative forcing and the indirect SST warming (Giannini 2010; Biasutti 2013; Gaetani et al. 2017; Mutton et al. 2022). However, this uncertainty is reduced in the latest CMIP6 models. A more robust increase of the NAFM rainfall accompanied with the strengthened monsoon westerly is projected (Jin et al. 2020; Wang et al. 2021), possibly because of the more significant warming over the Sahara. The substantial Sahara warming results in an intensified and a northward shift of Sahara low pressure (Biasutti 2013; Gaetani et al. 2017; Jin et al. 2020; Mutton et al. 2022), and this leads to a strengthened westerly over the North Africa and the weakened advection of the dry air into the monsoon region, which favors an increased monsoon rainfall.

Past climate is an effective reference to the future warming climate, which provides another perspective to understand the monsoon climate projection (Braconnot et al. 2012; Harrison et al. 2015; Tierney et al. 2020). The Last Interglacial (LIG; 127KaBP) and the Mid-Holocene (MH; 6KaBP) are the two warm interglacial epochs that have been widely studied. In these two epochs, the greenhouse gas levels are similar to that in preindustrial period, while the seasonality of the insolation is enhanced due to the perturbation of the Earth’s axis precession (Otto-Bliesner et al. 2017). The Earth receives more incoming solar radiation during boreal summer in LIG and MH compared to the glacial epochs and present climate (Otto-Bliesner et al. 2017). This results in a general warming over the Northern Hemisphere and a stronger interhemispheric thermal contrast (Braconnot et al. 2012; Zhao and Harrison 2012; Harrison et al. 2015; He and Zhou 2020), similar to the change pattern of the temperature contrast under global warming.

Evidences from both the proxy data and model simulation have demonstrated an increased AAM rainfall in interglacial epochs compared to the present climate (Weldeab et al. 2007; Tjallingii et al. 2008; Wang et al. 2008; Zhao and Harrison 2012; Zheng et al. 2013; Jiang et al. 2015; Shi and Yan 2019). It is suggested that the magnitude of the change of the natural forcing in the LIG and MH is comparable to that in the future global warming scenarios (Braconnot et al. 2012; Harrison et al. 2015). As an intensified AAM in both the interglacial epochs and global warming, one may wonder whether the mechanisms for this intensification are same under precession change or greenhouse induced climate warming. Few studies focus on this issue and connect the past change of AAM to the future warmer climate, which is benefit for the accurate monsoon projection. In the current study, we aim to give a comprehensive comparison of the

responses of AAM system to orbital perturbation and greenhouse induced climate warming based on a series of simulation from the latest CMIP6 models. The following questions are mainly to be addressed: 1) How does the AAM change in interglacial epochs (LIG and MH) and global warming in CMIP6 models? 2) What are the fundamental mechanisms for the change of AAM system? Three aspects of the AAM are investigated in the current study: monsoon rainfall, the regional low-level monsoon circulation (rotational component of the circulation) and the vertical motion (converge/divergence component of the circulation).

The rest of paper is organized as follow. Section 2 introduces the data and methods. Changes of AAM in interglacial epochs and global warming are compared in Section 3. Fundamental mechanisms for the change of AAM in different warming epochs are investigated in Section 4. The main conclusions are summarized in Section 5.

2 Data And Methods

2.1 Output from CMIP6 models

The monthly outputs from the following experiments are adopted for analyses: (1) The preindustrial control (PIC) experiment, which is performed under the fixed external forcing at preindustrial level and is integrated for hundreds of years (Eyring et al. 2016). (2) The lig127K (LIG) and mid-Holocene (MH) experiments, in which the levels of the greenhouse gas are similar to that in preindustrial period (Otto-Bliesner et al. 2017). Following Berger and Loutre (1991), the Earth's orbital parameters are prescribed in these two experiments to mimic the LIG and MH. (3) The shared socioeconomic pathway SSP5-8.5 experiment is adopted to represent the future warmer climate, in which the anthropogenic emission follows a high emission pathway toward 8.5 W m^{-2} in AD 2100 (O'Neill et al. 2016). (4) The abrupt-4xCO_2 experiment, in which the CO_2 concentration is abruptly quadrupled from preindustrial level and the model is integrated for 150 years, is further used to decompose the global warming induced climate response into fast (direct CO_2 radiative forcing) and slow (indirect SST warming) responses. The detailed information for each model used in this study is listed in Supplementary Table S1.

The last 50 years in the PIC simulation is adopted as the baseline climate in this study. The last 50 years in the LIG (MH) or SSP5-8.5 experiment is compared with the PIC experiment to extract the orbital perturbation or global warming induced climate change. All the model data are bilinearly interpolated onto a 2.5°×2.5° horizontal grid before analyses. The multi-model median (MMM) is used to evaluate the climate change, for the median is more robust to the outliers (Gleckler et al. 2008). According to Power et al. (2012), 68% intermodel agreement on the sign of the change equals the 95% confidence level based on the Student's t test. In the current study, a tighter threshold 70% intermodel agreement is adopted.

2.2 Definition of the Asian-African monsoon

The definition of the AAM region follows the concept of the global monsoon (Wang and Ding 2006; Wang and Ding 2008). The monsoon region should satisfy the following two criterions (Lee and Wang 2014):

(1) The local summer (May-September, MJJAS) precipitation minus the local winter (November-March, NDJFM) exceeds 2.5 mm day^{-1}; (2) The local summer precipitation contributes more than 55% to the annual precipitation. The Asian summer monsoon is further separated into the East Asian and the South Asian monsoons (Wang et al. 2003). The following three land monsoons are the focus of the current study: The East Asian monsoon (EAM), South Asian monsoon (SAM) and North African monsoon (NAFM).

2.3 Moisture budget for the change of monsoon rainfall

Moisture budget is performed to identify the dominant source for the change of monsoon rainfall. Based on Chou et al. (2009), the moisture budget equation can be written as:

$$P' = -\langle \omega \frac{\partial q}{\partial p} \rangle' - \langle \overrightarrow{v} \bullet \nabla q \rangle' + E' \quad (1)$$

where P, ω, q, $\overrightarrow{v}$ and E denotes the monsoon rainfall, vertical motion, specific humidity, horizontal circulation and evaporation respectively. The prime represents the orbital perturbation or global warming induced change of a variable, and the bracket represents the vertical integration from the surface to the top of the troposphere (200hPa). The three terms on the right side of the Eq. 1 denotes the monsoon rainfall change contributed by vertical moisture advection, horizontal moisture advection and evaporation respectively. It is suggested that the monsoon rainfall is largely dominated by the term of vertical moisture advection (also see the evaluation in Fig. 2) (e.g., Seager et al. 2010; Hsu et al. 2012; Huang and Xie 2015; He et al. 2020; Jiang et al. 2021), and the other two terms can be omitted. That is

$$P' \approx -\langle \omega \frac{\partial q}{\partial p} \rangle' \quad (2)$$

The vertical moisture advection term can be further decomposed into dynamic and thermodynamic term. Finally, one can obtain:

$$P' \approx -\langle \omega' \frac{\partial \bar{q}}{\partial p} \rangle - \langle \bar{\omega} \frac{\partial q'}{\partial p} \rangle \quad (3)$$

3 Changes Of Asian-african Monsoon In Interglacial Epochs And Global Warming Scenario

To investigate the changes of AAM in interglacial epochs and global warming, the MMM-simulated changes of precipitation and wind at 850hPa are shown in Fig. 1. In the LIG, increased rainfall is found over the land monsoon region. While decreased rainfall is seen over the vast area of ocean, especially over the tropical ocean (Fig. 1a). The “wet land-dry ocean” pattern indicates a shift of the convection to the land. The monsoon area expands northward (Fig. 1a), suggesting a strengthening and northward shift of the AAM system. From a large-scale perspective, the low-level wind is characterized by a cyclone

anomaly, which covers subtropical North Africa to East Asia (Fig. 1a). Westerly anomalies prevail from the tropical Atlantic to North Africa and strengthens the climatological NAFM circulation. Easterly anomalies cover the tropical northern Indian Ocean (IO) where the climatological maximum westerly locates, implying a weakening of the SAM circulation. This flow turns northward at the eastern IO and becomes westerly over the Southern TP. East Asia is featured by the southerly anomalies, implying a strengthening of the EAM circulation. Except for the smaller changes in magnitude, change of the spatial pattern of the precipitation and low-level wind in the MH (Fig. 1b) is almost the same as that in the LIG (Fig. 1a). Compared to the previous generations of the climate models, the simulated feature of the AAM in interglacial epochs by CMIP6 models are similar to CMIP3/5 models (Zhao and Harrison 2012; Zheng et al. 2013; Kelly et al. 2018; D'Agostino et al. 2019).

Figure 1c depicts the change of AAM in SSP5-8.5 experiment. Similar as in the interglacial epochs, the land monsoon rainfall over the AAM region increases under the global warming scenario, and the low-level wind is also featured by a continental cyclone anomaly over the Eurasian continent. The precipitation also increases over a vast area in the surrounding oceans under the global warming scenario, especially over the tropical and North Pacific, which is different from the interglacial epochs (Fig. 1a, b). In general, the characteristics of the changes of continental monsoon rainfall and low-level circulation in SSP5-8.5 share similar pattern with that in the LIG and MH.

A set of monsoon metrics is defined to quantitatively measure the changes of monsoon rainfall and low-level circulation in different warming epochs. Monsoon rainfall indices (i.e., P_EA, P_SA and P_NAF) are defined by the regional averaged monsoon rainfall over monsoon domains. The EAM circulation index (C_EA) is defined by the averaged meridional wind (V at 850hPa) over East Asia (20°N-45°N, 110°E-125°E) (He et al. 2019; Li et al. 2019; He and Zhou 2020). The SAM circulation index (C_SA) is defined by the intensity of the westerly over tropical northern IO (2.5°N-15°N, 55°E-100°E) where the climatological maximum westerlies locate (Li et al. 2022). Following Jin et al. (2020), the NAFM circulation index (C_NAF) is defined as the regional averaged westerly over North Africa (0-12.5°N, 37.5°W-22.5°E). Changes of the metrics are shown in Fig. 2. The robustly increased monsoon rainfall in interglacial epochs and global warming scenario is confirmed by the positive changes of monsoon rainfall indices (Fig. 2a). The C_EA and C_NAF are robustly increased in the LIG, MH and SSP5-8.5 experiment (Fig. 2b), indicating a robust strengthening of the EAM and NAFM circulation. And the C_SA is significantly decreased in all the three experiments (Fig. 3b), demonstrating a robust weakening of the SAM circulation.

The above analyses seem to support that the changes of AAM in interglacial epochs and global warming scenario are similar in the spatial pattern, despite of the differential changes in magnitude (Fig. 2). It is suggested that change of the monsoon rainfall results from the combined effect of the dynamic and thermodynamic processes (Held and Soden 2006; Chou et al. 2009; Hsu et al. 2012; Seager et al. 2010; He et al. 2020; Jiang et al. 2021). To test the possibly different contributions by thermodynamic and dynamic terms, the moisture budget based on Eq. 3 is performed. As shown in Fig. 3, the increased monsoon rainfall in interglacial epochs is primarily attributed to the dynamic process (blue bars in

Fig. 3a, b), with a modest contribution of the thermodynamic process (orange bars in Fig. 3a, b). On the contrary, under global warming, the dynamic process suppresses the monsoon convection (blue bars in Fig. 3c), but the thermodynamic process associated with the increased mean moisture overwhelms the effect of dynamic term and results in the increase of monsoon rainfall (orange bars in Fig. 3c).

As the change in vertical velocity is responsible for the dynamic term of precipitation change, Fig. 4 shows the MMM-simulated changes of vertical velocity at 500hPa. Substantial ascending anomalies are found over the land monsoon region in the LIG and MH (Fig. 4a, b). In sharp contrast, the land monsoon region is featured by descending anomalies in SSP5-8.5 scenario (Fig. 4c). Figure 4d shows the changes in vertical motion indices (VWI), defined as the regional averaged vertical motion at 500hPa within EAM, SAM and NAFM regions. It shows that the vertical ascending motion is strengthened over all these three regions during interglacial epochs (dark blue and light blue bars), but weakened under SSP5-8.5 scenario (red bars). The strengthened monsoon ascending motion in interglacial epochs leads to the dynamic increase of the monsoon rainfall, while the weakened monsoon ascending motion under global warming scenario acts to suppress monsoon rainfall.

The qualitative and quantitative analyses demonstrate that the AAM rainfall increases in both interglacial epochs and global warming, accompanied with the similar change of low-level monsoon circulation but different change of vertical motion. The moisture budget analysis suggests that the increased monsoon rainfall is dominated by the dynamic process associated with the strengthened ascending motion in interglacial epochs but dominated by the thermodynamic process due to the increased mean moisture under global warming. Based on the simulation from CMIP6 models, our analyses and diagnoses demonstrate that the change of AAM in interglacial epochs is not an analogue of that under global warming, consistent with previous studies based on the CMIP5 models or a single model simulation (D'Agostino et al. 2019; Shi and Yan 2019).

4 Mechanisms For The Change Of Asian-african Monsoon In Interglacial Epochs And Global Warming

Observational analyses and modeled evidences have suggested that the land-ocean thermal contrast is essential for the formation and evolution of the AAM (Li and Yanai 1996; Sun et al. 2010; Wang and LinHo 2002; Dai et al. 2013; Kamae et al. 2014). In the LIG and MH, the marked feature in surface temperature is the profound warming over the Eurasian and North African continent, while the SST change is negligible (Fig. 5a, b). Under global warming scenario, the ocean significantly warms up in addition to the continental warming (Fig. 5c). The profound global SST warming may weaken the monsoon by reducing the land-ocean thermal contrast (Shaw and Voigt 2015; He and Zhou 2020) and enhancing the atmospheric static stability (Kitoh et al. 2013; Kamae et al. 2014; Lee and Wang 2014; Wang et al. 2020a; Wang et al. 2021), and may be essential for the distinction of the AAM in between global warming and interglacial epochs.

4.1 Fast and slow responses of AAM to global warming

The idealized abrupt-4xCO_2 experiment performed by CMIP6 models is analyzed in this section (see Section 2a), to separate the monsoon response to global warming into the direct effect of CO_2 radiative forcing and the indirect effect of SST warming, known as the fast and slow responses respectively. Following previous studies (Bony et al. 2013; He et al. 2020), the fast response is defined as the difference between the 1st year in the abrupt-4xCO_2 experiment and the last 50 years in the PIC experiment, and the slow response is defined as the difference between the last 50 years and 1st year in the abrupt-4xCO_2 experiment. The responses of surface temperature, precipitation and vertical velocity are shown in Figs. 5–7, with regional averaged moisture budget analysis (Fig. 7e, f). This idealized simulation can basically reproduce the projected change of the AAM in the scenario experiment (comparing the Fig. 1c and Fig. 6c), suggesting that the decomposition based on the abrupt-4xCO_2 experiment is reasonable.

Under the direct CO_2 radiative forcing, substantial surface warming is seen over Eurasian continent but the increase of SST is much weaker (Fig. 5d), and rainfall increases over the land monsoon region (Fig. 6a) accompanied with the strengthened ascending motion (Fig. 7a, d). The precipitation decreases over the ocean (Fig. 6a), possibly due to the stabilization of the boundary layer (Cao et al. 2012; He and Soden 2015; Richardson et al. 2016). The rainfall change exhibits a “wet land-dry ocean” pattern, similar to that in the interglacial epochs (Fig. 1a, b). Similar to the dominant control of dynamic term on precipitation, the moisture budget in the fast response demonstrates that the dynamic process contributes a large fraction for the increased monsoon rainfall in addition to the thermodynamic process (Fig. 7e), consistent with Bony et al. (2013) which emphasizes the importance of dynamic modulation of the tropical precipitation under direct CO_2 radiative forcing. The low-level monsoon circulation is characterized by a large-scale cyclonic flow surrounding the Eurasian continent (Fig. 6a). These features imply a shift of the convection to the land and an overall strengthening of the AAM system, which is generally the same as in the interglacial epochs (Fig. 1a, b). Similarity between the fast response and interglacial epochs is also found in the change of each regional monsoon system (comparing the changes of monsoon metrics in Fig. 2 and Supplementary Fig. S1), suggesting that the change of AAM in the fast response is an analogue of that in the interglacial epoch.

In the slow response, the low-level monsoon circulation (Fig. 6b; Supplementary Fig. S1) and the climatological monsoon ascending motion (Fig. 7b, d) show an overall weakening, differing markedly from the fast response and interglacial epochs. The land monsoon rainfall increases over the Asian monsoon region but decreases over the NAFM region (Fig. 6b; Supplementary Fig. S1). It is due to the competition between the dynamic and thermodynamic processes that leads to the inconsistent change of the regional monsoon rainfall (Fig. 7f). Over the surrounding ocean, substantially increased rainfall is found, except for the Maritime Continent and tropical North Atlantic, sharing similar pattern with the scenario experiment (Fig. 1c). The above results suggest that the change of AAM in the slow response is completely different from the fast response and the interglacial epochs, and it is responsible for the different changes of AAM in between the interglacial epochs and global warming scenario.

By decomposing the total response to global warming into the effects of CO_2 direct radiative forcing and indirect SST warming, the above analyses and diagnoses demonstrate that the change of the AAM in interglacial epoch is an analogue of the effect of CO_2 direct forcing instead of the total effect of global warming. The SST warming further mediates the AAM and largely explains the distinction of the AAM in between the interglacial epochs and global warming.

4.2 Thermal control on the monsoon response

In interglacial epochs, the profound warming over the Eurasian continent significantly decreases the sea level pressure (SLP), and a continental cyclone anomaly is stimulated over the Eurasian land (contours in Fig. 5a, b). As a part of this anomalous cyclone, the westerly anomaly over North Africa and the southerly anomaly over East Asia strengthen the NAFM and EAM circulation respectively. Observational and theoretical analyses have demonstrated that monsoon intensity is closely related to surface equivalent potential temperature (θ_e) rather than surface temperature (Nie et al. 2010; Shaw and Voigt 2015; Zhou and Xie 2018; Hill 2019; Seth et al. 2019; Song et al. 2022), θ_e is thus adopted to evaluate the change of land-ocean thermal contrast. Figure 8 examines the changes in specific humidity and θ_e at surface. A profound increase of θ_e is seen over the AAM region during the interglacial epochs (Fig. 8a, b) and in the fast response to global warming (Fig. 8d), characterized by a belt of higher θ_e extending from the North Africa to East Asia. This belt of higher θ_e is contributed by both increased temperature and humidity (Fig. 8a, b, d), and the latter is contributed by the continental cyclone anomaly (Fig. 5a, b) which transports air mass with higher moisture from the tropical ocean into the land monsoon region. As the monsoon rainfall follows higher near-surface θ_e (Nie et al. 2010; Hill 2019; Seth et al. 2019), a higher increase of θ_e over the AAM region and an enhanced land-ocean θ_e contrast favor the enhanced monsoon convection (Neelin 2007; Shaw and Voigt 2015; Zhou and Xie 2018), with strengthened monsoon ascending motion and increased monsoon rainfall during the interglacial epochs and the simulated fast response to global warming. The horizontal monsoon circulation is also strengthened except the SAM due to a remote forcing from the increased North African monsoon rainfall (Li et al. 2022; see the discussion in Section 5).

In the slow response, although the amplitude of ocean warming is smaller than the land in terms of surface temperature (Fig. 5e), higher increase of θ_e is seen over the tropical and subtropical ocean, and the land-ocean θ_e contrast is decreased (Fig. 8c). This is because of the smaller increase of specific humidity over the continent than the ocean (contours in Fig. 8e), due to the limited capacity of evaporation over land (Byrne and O'Gorman 2013). As a result, the land-ocean θ_e contrast is also decreased in the total response and the SSP5-8.5 scenario (Fig. 8c, f), which favors a weakening of the AAM system under global warming background.

As previous studies emphasized the role of atmospheric static stability in the weakened ascending motion over global monsoon regions under global warming (Kitoh et al. 2013; Lee and Wang 2014; Wang et al. 2020a; Wang et al. 2021), the change in static stability is examined in Fig. 9 in terms of the vertical temperature profile over the land monsoon region. In the slow response and the SSP5-8.5 scenario, the

atmosphere warms up profoundly with stronger warming in the upper troposphere than the lower troposphere (Fig. 9), leading to a robustly enhanced atmospheric static stability. The enhanced static stability in the slow response acts to weaken the climatological ascending motion (Fig. 7b). In interglacial epochs and in the fast response to increased CO_2 forcing, the static stability keeps generally unchanged (Fig. 9) and cannot weaken the vertical monsoon motion. With the higher near-surface θ_e and the enhanced land-ocean θ_e contrast, the ascending motion is strengthened. In all, the existence of substantial stabilization depends on whether there is sufficient oceanic warming (comparing the dashed red and blue lines in Fig. 9). Through the moist adiabatic adjustment process (Knutson and Manabe 1995; Seager et al. 2010; Wang et al. 2020b; Wang et al. 2020c), the SST warming is responsible for the enhanced atmospheric static stability under global warming, as well as the weakening of the monsoon ascending motion under greenhouse gases forcing (see the quantitative evaluation in Fig. 4d).

The climate change in interglacial epoch is ultimately modulated by the enhanced seasonal cycle of the solar radiation. The Earth receives more (less) incoming solar radiation during boreal summer (winter), with almost unchanged intensity of the annual mean solar radiation (Otto-Bliesner et al. 2017). Due to the larger thermal inertia of the ocean, the SST remains almost unchanged throughout the year while the land warms significantly during boreal summer in interglacial epochs, leading to an enhanced land-ocean θ_e contrast and the strengthening of the AAM system. Since the increased greenhouse gases heat the surface throughout the year, both the land and ocean profoundly warm up. The ocean warming decreases the land-ocean θ_e contrast and enhances the tropospheric static stability, which offsets the enhancement of AAM system. It is the nature of the external forcing that determines the response of the AAM system in the interglacial epochs and global warming.

5 Summary And Discussion

The Asian-African monsoon (AAM) is the crucial system in the Northern Hemisphere, the variability of which greatly impacts the hydrological cycle. Based on a series of simulation from latest CMIP6 models, changes of the AAM in interglacial epochs [Last Interglacial (LIG) and Mid-Holocene (MH)] are compared to that under global warming, to understand the response of the AAM to orbital forcing and greenhouse induced climate warming. The response of the AAM to global warming is further decomposed into the direct effect of CO_2 radiative forcing and the indirect effect of SST warming, to address the mechanism for the different response of AAM to global warming compared with its change in the interglacial epochs. The major findings are summarized as follows.

1) The AAM rainfall is identified to increase in both interglacial epochs and global warming, accompanied with the similar change of low-level monsoon circulation. However, the increased monsoon rainfall primarily results from the dynamic (thermodynamic) process in interglacial epochs (global warming) associated with the strengthened monsoon circulation (increased mean moisture), suggesting that the interglacial epoch is not an analogue of the AAM response to global warming. With the aid of the decomposition of the fast (direct CO_2 radiative forcing) and slow (indirect SST warming) responses to global warming, further analyses show evidences that the interglacial epoch is similar to the fast

response of AAM to increased CO_2 forcing under global warming, and SST warming further mediates the AAM and causes the distinctive responses in between the interglacial epochs and global warming. Change of the AAM can be explained by the change of land-ocean θ_e contrast. The specific physical mechanisms for the change of AAM are summarized in the schematic diagram of Fig. 10.

2) In interglacial epochs, incoming solar radiation to the northern hemisphere is intensified in boreal summer. Forced by the enlarged seasonal cycle of incoming solar radiation, the land at northern hemisphere warms up in boreal summer while the SST change is negligible. The profound Eurasian warming induces a local continental-scale cyclone anomaly (Fig. 10a), and results in the strengthening of the low-level EAM and NAFM circulation. The higher mean moisture from the tropical ocean is transported into the land monsoon region, which profoundly increases the local humidity and θ_e. With an enlarged land-ocean θ_e contrast and an almost unchanged atmospheric static stability, the climatological ascending motion is strengthened (Fig. 10a). As a result, the monsoon rainfall is dynamically increased.

3) Under global warming, the direct CO_2 radiative forcing acts to enhance AAM through a similar mechanism as in interglacial epochs, but the indirect effect of global SST warming acts to weaken AAM and is responsible for the distinctive AAM changes under global warming. The substantial global SST warming, which is absent in interglacial epochs, reduces the magnitude of the intensification of AAM by decreasing land-ocean θ_e contrast and enhancing tropospheric static stability (Fig. 10b). The weakened land-ocean θ_e contrast is due to the combined effect of the change in temperature and specific humidity associated with SST warming. The weakened land-ocean θ_e contrast and enhanced static stability both tend to suppress the monsoon rainfall, while the thermodynamic process associated the increased mean moisture compensates the negative dynamic effect and results in a net increase of monsoon rainfall.

This work mainly focuses on the entire AAM system, though regional difference exists within the AAM domain. Different from the strengthened EAM and NAFM circulation, the low-level SAM circulation is weakened in both interglacial epochs and global warming scenario (Fig. 2b; Supplementary Fig. S1b). The regional difference primarily results from the interplay among the regional monsoon systems and the SST warming pattern. In interglacial epochs and in response to direct CO_2 forcing, the westerly horizontal wind of SAM circulation is weakened by the enhanced latent heating over NAFM region as a Kelvin wave response (Fig. 10a) (Li et al. 2022). Under global warming scenario, the weakening of the SAM westerly is largely attributed to the slow El Niño-like oceanic warming pattern over the equatorial Pacific associated with the weakened Walker circulation and suppressed convection over the Maritime Continent (Fig. 10b) (Li et al. 2022), in addition to weakened land-ocean θ_e contrast and enhanced static stability. Nevertheless, the change in the vertical monsoon circulation and precipitation are coherent among the EAM, SAM and NAFM regions.

The current study indicates that the future monsoon change involves more complicated processes than that in the interglacial epochs. The results highlight that the SST warming under global warming scenario is the key for the distinctive changes of AAM in between interglacial epochs and global warming, and accurate projection of the pattern and amplitude of the SST warming is required for future monsoon

climate projection (Chen and Zhou 2015; Li et al. 2017a; Xie et al. 2015). However, large uncertainty of global warming induced SST change still exists among the current state-of-art climate models (Xie et al. 2015), for example, an El Niño-like or a La Niña-like SST warming pattern over the equatorial Pacific (Coats and Karnauskas 2017; Li et al. 2016; Seager et al. 2019). Great effort is required to narrow this uncertainty and give a more accurate monsoon projection in the future work.

Declarations

Acknowledgments

The authors wish to acknowledge all the modeling groups for providing the model outputs.

Authors' Contributions

Y. W., C. H. and T. L. designed the research. Y. W. performed the analysis and plotted the figures. Y. W. drafted the manuscript, C. H., T. L., C. Z. and X. G. provided the comments and revised the manuscript.

Funding

This work was supported by the National Natural Science Foundation of China (42088101).

Data availability

All the data used in this study are publicly available. The CMIP6 model data are available at https://esgf-node.llnl.gov.

Competing interests

The authors declare no conflicts of interest or competing interests.

Conflict of interest

The authors have no relevant financial or non-financial interests to disclose.

Ethical approval

Not applicable.

Consent to participate

Not applicable.

Consent for publication

Not applicable.

References

1. Berger A, Loutre MF (1991) Insolation values for the climate of the last 10 million years. Quaternary Science Reviews 10:297-317 doi:https://doi.org/10.1016/0277-3791(91)90033-Q
2. Biasutti M (2013) Forced Sahel rainfall trends in the CMIP5 archive. Journal of Geophysical Research: Atmospheres 118:1613-1623 doi:https://doi.org/10.1002/jgrd.50206
3. Bony S, Bellon G, Klocke D, Sherwood S, Fermepin S, Denvil S (2013) Robust direct effect of carbon dioxide on tropical circulation and regional precipitation. Nature Geoscience 6:447-451 doi:10.1038/ngeo1799
4. Braconnot P et al. (2012) Evaluation of climate models using palaeoclimatic data. Nature Climate Change 2:417-424 doi:10.1038/nclimate1456
5. Byrne MP, O'Gorman PA (2013) Land–Ocean Warming Contrast over a Wide Range of Climates: Convective Quasi-Equilibrium Theory and Idealized Simulations. Journal of Climate 26:4000-4016 doi:10.1175/JCLI-D-12-00262.1
6. Cao J, Wang B, Wang B, Zhao H, Wang C, Han Y (2020) Sources of the Intermodel Spread in Projected Global Monsoon Hydrological Sensitivity. Geophysical Research Letters 47:e2020GL089560 doi:https://doi.org/10.1029/2020GL089560
7. Cao L, Bala G, Caldeira K (2012) Climate response to changes in atmospheric carbon dioxide and solar irradiance on the time scale of days to weeks. Environmental Research Letters 7:034015 doi:10.1088/1748-9326/7/3/034015
8. Chen X, Zhou T (2015) Distinct effects of global mean warming and regional sea surface warming pattern on projected uncertainty in the South Asian summer monsoon. 42:9433-9439 doi:10.1002/2015gl066384
9. Chou C, Neelin JD, Chen C-A, Tu J-Y (2009) Evaluating the "Rich-Get-Richer" Mechanism in Tropical Precipitation Change under Global Warming. Journal of Climate 22:1982-2005 doi:10.1175/2008JCLI2471.1
10. Coats S, Karnauskas KB (2017) Are Simulated and Observed Twentieth Century Tropical Pacific Sea Surface Temperature Trends Significant Relative to Internal Variability? Geophysical Research Letters 44:9928-9937 doi:https://doi.org/10.1002/2017GL074622
11. D'Agostino R, Bader J, Bordoni S, Ferreira D, Jungclaus J (2019) Northern Hemisphere Monsoon Response to Mid-Holocene Orbital Forcing and Greenhouse Gas-Induced Global Warming. Geophysical Research Letters 46:1591-1601 doi:https://doi.org/10.1029/2018GL081589
12. Dai A, Li H, Sun Y, Hong L-C, LinHo, Chou C, Zhou T (2013) The relative roles of upper and lower tropospheric thermal contrasts and tropical influences in driving Asian summer monsoons. Journal of Geophysical Research: Atmospheres 118:7024-7045 doi:10.1002/jgrd.50565
13. Eyring V, Bony S, Meehl GA, Senior CA, Stevens B, Stouffer RJ, Taylor KE (2016) Overview of the Coupled Model Intercomparison Project Phase 6 (CMIP6) experimental design and organization. Geosci Model Dev 9:1937-1958 doi:10.5194/gmd-9-1937-2016

14. Gadgil S, Rupa Kumar K (2006) The Asian monsoon — agriculture and economy. In: The Asian Monsoon. Springer Berlin Heidelberg, Berlin, Heidelberg, pp 651-683. doi:10.1007/3-540-37722-0_18
15. Gaetani M et al. (2017) West African monsoon dynamics and precipitation: the competition between global SST warming and CO2 increase in CMIP5 idealized simulations. Climate Dynamics 48:1353-1373 doi:10.1007/s00382-016-3146-z
16. Giannini A (2010) Mechanisms of Climate Change in the Semiarid African Sahel: The Local View. Journal of Climate 23:743-756 doi:10.1175/2009jcli3123.1
17. Harrison SP et al. (2015) Evaluation of CMIP5 palaeo-simulations to improve climate projections. Nature Climate Change 5:735-743 doi:10.1038/nclimate2649
18. He C, Li T, Zhou W (2020) Drier North American Monsoon in Contrast to Asian–African Monsoon under Global Warming. Journal of Climate 33:9801-9816 doi:10.1175/jcli-d-20-0189.1
19. He C, Wang Z, Zhou T, Li T (2019) Enhanced Latent Heating over the Tibetan Plateau as a Key to the Enhanced East Asian Summer Monsoon Circulation under a Warming Climate. Journal of Climate 32:3373-3388 doi:10.1175/JCLI-D-18-0427.1
20. He C, Zhou W (2020) Different Enhancement of the East Asian Summer Monsoon under Global Warming and Interglacial Epochs Simulated by CMIP6 Models: Role of the Subtropical High. Journal of Climate 33:9721-9733 doi:10.1175/jcli-d-20-0304.1
21. He J, Soden BJ (2015) Anthropogenic Weakening of the Tropical Circulation: The Relative Roles of Direct CO2 Forcing and Sea Surface Temperature Change. Journal of Climate 28:8728-8742 doi:10.1175/jcli-d-15-0205.1
22. Held IM, Soden BJ (2006) Robust Responses of the Hydrological Cycle to Global Warming. Journal of Climate 19:5686-5699 doi:10.1175/JCLI3990.1
23. Hill SA (2019) Theories for Past and Future Monsoon Rainfall Changes. Current Climate Change Reports 5:160-171 doi:10.1007/s40641-019-00137-8
24. Hsu P-c, Li T (2012) Is “rich-get-richer” valid for Indian Ocean and Atlantic ITCZ? Geophysical Research Letters 39 doi:10.1029/2012gl052399
25. Hsu P-c, Li T, Luo J-J, Murakami H, Kitoh A, Zhao M (2012) Increase of global monsoon area and precipitation under global warming: A robust signal? Geophysical Research Letters 39 doi:10.1029/2012gl051037
26. Huang P, Xie S-P (2015) Mechanisms of change in ENSO-induced tropical Pacific rainfall variability in a warming climate. Nature Geoscience 8:922-926 doi:10.1038/ngeo2571
27. IPCC (2013) Climate Change 2013: The Physical Science Basis. Contribution of Working Group I to the Fifth Assessment Report of the Intergovernmental Panel on Climate Change. Cambridge University Press, Cambridge, United Kingdom and New York, NY, USA. doi:10.1017/CBO9781107415324
28. Jiang D, Tian Z, Lang X (2015) Mid-Holocene global monsoon area and precipitation from PMIP simulations. Climate Dynamics 44:2493-2512 doi:10.1007/s00382-014-2175-8

29. Jiang Z, Hou Q, Li T, Liang Y, Li L (2021) Divergent Responses of Summer Precipitation in China to 1.5°C Global Warming in Transient and Stabilized Scenarios. Earth's Future 9:e2020EF001832 doi:https://doi.org/10.1029/2020EF001832
30. Jin C, Wang B, Liu J (2020) Future Changes and Controlling Factors of the Eight Regional Monsoons Projected by CMIP6 Models. Journal of Climate 33:9307-9326 doi:10.1175/jcli-d-20-0236.1
31. Jones GS, Stott PA, Christidis N (2013) Attribution of observed historical near–surface temperature variations to anthropogenic and natural causes using CMIP5 simulations. Journal of Geophysical Research: Atmospheres 118:4001-4024 doi:https://doi.org/10.1002/jgrd.50239
32. Kamae Y, Watanabe M, Kimoto M, Shiogama H (2014) Summertime land–sea thermal contrast and atmospheric circulation over East Asia in a warming climate—Part I: Past changes and future projections. Climate Dynamics 43:2553-2568 doi:10.1007/s00382-014-2073-0
33. Kelly P, Kravitz B, Lu J, Leung LR (2018) Remote Drying in the North Atlantic as a Common Response to Precessional Changes and CO2 Increase Over Land. Geophysical Research Letters 45:3615-3624 doi:https://doi.org/10.1002/2017GL076669
34. Kitoh A, Endo H, Krishna Kumar K, Cavalcanti IFA, Goswami P, Zhou T (2013) Monsoons in a changing world: A regional perspective in a global context. Journal of Geophysical Research: Atmospheres 118:3053-3065 doi:10.1002/jgrd.50258
35. Knutson TR, Manabe S (1995) Time-Mean Response over the Tropical Pacific to Increased C02 in a Coupled Ocean-Atmosphere Model. Journal of Climate 8:2181-2199 doi:10.1175/1520-0442(1995)008<2181:TMROTT>2.0.CO;2
36. Kucharski F, Bracco A, Yoo JH, Tompkins AM, Feudale L, Ruti P, Dell'Aquila A (2009) A Gill–Matsuno-type mechanism explains the tropical Atlantic influence on African and Indian monsoon rainfall. Quarterly Journal of the Royal Meteorological Society 135:569-579 doi:https://doi.org/10.1002/qj.406
37. Lee J-Y, Wang B (2014) Future change of global monsoon in the CMIP5. Climate Dynamics 42:101-119 doi:10.1007/s00382-012-1564-0
38. Li C, Yanai M (1996) The Onset and Interannual Variability of the Asian Summer Monsoon in Relation to Land–Sea Thermal Contrast. Journal of Climate 9:358-375 doi:10.1175/1520-0442(1996)009<0358:TOAIVO>2.0.CO;2
39. Li G, Xie S-P, Du Y, Luo Y (2016) Effects of excessive equatorial cold tongue bias on the projections of tropical Pacific climate change. Part I: the warming pattern in CMIP5 multi-model ensemble. Climate Dynamics 47:3817-3831 doi:10.1007/s00382-016-3043-5
40. Li G, Xie S-P, He C, Chen Z (2017a) Western Pacific emergent constraint lowers projected increase in Indian summer monsoon rainfall. Nature Climate Change 7:708-712 doi:10.1038/nclimate3387
41. Li T et al. (2022) Distinctive South and East Asian monsoon circulation responses to global warming. Science Bulletin 67:762-770 doi:https://doi.org/10.1016/j.scib.2021.12.001
42. Li X, Ting M, Li C, Henderson N (2015) Mechanisms of Asian Summer Monsoon Changes in Response to Anthropogenic Forcing in CMIP5 Models. Journal of Climate. 28:4107-4125

doi:10.1175/jcli-d-14-00559.1

43. Li Y, Ding Y, Li W (2017b) Interdecadal variability of the Afro-Asian summer monsoon system. Advances in Atmospheric Sciences 34:833-846 doi:10.1007/s00376-017-6247-7
44. Li Z, Sun Y, Li T, Chen W, Ding Y (2021) Projections of South Asian Summer Monsoon under Global Warming from 1.5° to 5°C. Journal of Climate 34:7913-7926 doi:10.1175/jcli-d-20-0547.1
45. Li Z, Sun Y, Li T, Ding Y, Hu T (2019) Future Changes in East Asian Summer Monsoon Circulation and Precipitation Under 1.5 to 5 °C of Warming. Earth's Future 7:1391-1406 doi:10.1029/2019ef001276
46. Liu Y, Chiang JCH, Chou C, Patricola CM (2014) Atmospheric teleconnection mechanisms of extratropical North Atlantic SST influence on Sahel rainfall. Climate Dynamics 43:2797-2811 doi:10.1007/s00382-014-2094-8
47. Mall RK, Singh R, Gupta A, Srinivasan G, Rathore LS (2006) Impact of Climate Change on Indian Agriculture: A Review. Climatic Change 78:445-478 doi:10.1007/s10584-005-9042-x
48. Menon A, Levermann A, Schewe J, Lehmann J, Frieler K (2013) Consistent increase in Indian monsoon rainfall and its variability across CMIP-5 models. Earth Syst Dynam 4:287-300 doi:10.5194/esd-4-287-2013
49. Mutton H, Chadwick R, Collins M, Lambert FH, Geen R, Todd A, Taylor CM (2022) The Impact of the Direct Radiative Effect of Increased CO2 on the West African Monsoon. Journal of Climate 35:2441-2458 doi:10.1175/jcli-d-21-0340.1
50. Nie J, Boos WR, Kuang Z (2010) Observational Evaluation of a Convective Quasi-Equilibrium View of Monsoons. Journal of Climate 23:4416-4428 doi:10.1175/2010jcli3505.1
51. Neelin JD (2007) Moist dynamics of tropical convection zones in monsoons, teleconnections and global warming. The Global Circulation of the Atmosphere Schneider T and Sobel AH, Eds, Princeton University Press, 267–301.
52. O'Neill BC et al. (2016) The Scenario Model Intercomparison Project (ScenarioMIP) for CMIP6. Geosci Model Dev 9:3461-3482 doi:10.5194/gmd-9-3461-2016
53. Otto-Bliesner BL et al. (2017) The PMIP4 contribution to CMIP6 – Part 2: Two interglacials, scientific objective and experimental design for Holocene and Last Interglacial simulations. Geosci Model Dev 10:3979-4003 doi:10.5194/gmd-10-3979-2017
54. Power SB, Delage F, Colman R, Moise A (2012) Consensus on Twenty-First-Century Rainfall Projections in Climate Models More Widespread than Previously Though. Journal of Climate 25:3792-3809 doi:10.1175/jcli-d-11-00354.1
55. Richardson TB, Forster PM, Andrews T, Parker DJ (2016) Understanding the Rapid Precipitation Response to CO2 and Aerosol Forcing on a Regional Scale. Journal of Climate 29:583-594 doi:10.1175/jcli-d-15-0174.1
56. Seager R, Cane M, Henderson N, Lee D-E, Abernathey R, Zhang H (2019) Strengthening tropical Pacific zonal sea surface temperature gradient consistent with rising greenhouse gases. Nature Climate Change 9:517-522 doi:10.1038/s41558-019-0505-x

57. Seager R, Naik N, Vecchi GA (2010) Thermodynamic and Dynamic Mechanisms for Large-Scale Changes in the Hydrological Cycle in Response to Global Warming. Journal of Climate 23:4651-4668 doi:10.1175/2010jcli3655.1
58. Seth A, Giannini A, Rojas M, Rauscher SA, Bordoni S, Singh D, Camargo SJ (2019) Monsoon Responses to Climate Changes—Connecting Past, Present and Future. Current Climate Change Reports 5:63-79 doi:10.1007/s40641-019-00125-y
59. Sharmila S, Joseph S, Sahai AK, Abhilash S, Chattopadhyay R (2015) Future projection of Indian summer monsoon variability under climate change scenario: An assessment from CMIP5 climate models. Global and Planetary Change 124:62-78 doi:https://doi.org/10.1016/j.gloplacha.2014.11.004
60. Shaw TA, Voigt A (2015) Tug of war on summertime circulation between radiative forcing and sea surface warming. Nature Geoscience 8:560-566 doi:10.1038/ngeo2449
61. Shi J, Yan Q (2019) Evolution of the Asian–African Monsoonal Precipitation over the last 21 kyr and the Associated Dynamic Mechanisms. Journal of Climate 32:6551-6569 doi:10.1175/jcli-d-19-0074.1
62. Song F, Zhang GJ, Ramanathan V, Leung LR (2022) Trends in surface equivalent potential temperature: A more comprehensive metric for global warming and weather extremes. Proceedings of the National Academy of Sciences 119:e2117832119 doi:doi:10.1073/pnas.2117832119
63. Sooraj KP, Terray P, Mujumdar M (2015) Global warming and the weakening of the Asian summer monsoon circulation: assessments from the CMIP5 models. Climate Dynamics 45:233-252 doi:10.1007/s00382-014-2257-7
64. Sun Y, Ding Y (2010) A projection of future changes in summer precipitation and monsoon in East Asia. Science China Earth Sciences 53:284-300 doi:10.1007/s11430-009-0123-y
65. Sun Y, Ding Y, Dai A (2010) Changing links between South Asian summer monsoon circulation and tropospheric land-sea thermal contrasts under a warming scenario. Geophysical Research Letters 37 doi:10.1029/2009gl041662
66. Sutton RT, Dong B, Gregory JM (2007) Land/sea warming ratio in response to climate change: IPCC AR4 model results and comparison with observations. Geophysical Research Letters 34 doi:https://doi.org/10.1029/2006GL028164
67. Tierney JE et al. (2020) Past climates inform our future. Science 370:eaay3701 doi:doi:10.1126/science.aay3701
68. Tjallingii R et al. (2008) Coherent high- and low-latitude control of the northwest African hydrological balance. Nature Geoscience 1:670-675 doi:10.1038/ngeo289
69. Turner AG, Annamalai H (2012) Climate change and the South Asian summer monsoon. Nature Climate Change 2:587-595 doi:10.1038/nclimate1495
70. Ueda H, Iwai A, Kuwako K, Hori ME (2006) Impact of anthropogenic forcing on the Asian summer monsoon as simulated by eight GCMs. Geophysical Research Letters 33 doi:10.1029/2005gl025336
71. Wang B et al. (2021) Monsoons Climate Change Assessment. Bulletin of the American Meteorological Society 102:E1-E19 doi:10.1175/bams-d-19-0335.1

72. Wang B, Clemens SC, Liu P (2003) Contrasting the Indian and East Asian monsoons: implications on geologic timescales. Marine Geology 201:5-21 doi:https://doi.org/10.1016/S0025-3227(03)00196-8
73. Wang B, Ding Q (2006) Changes in global monsoon precipitation over the past 56 years. Geophysical Research Letters 33 doi:https://doi.org/10.1029/2005GL025347
74. Wang B, Ding Q (2008) Global monsoon: Dominant mode of annual variation in the tropics. Dynamics of Atmospheres and Oceans 44:165-183 doi:https://doi.org/10.1016/j.dynatmoce.2007.05.002
75. Wang B, Jin C, Liu J (2020a) Understanding Future Change of Global Monsoons Projected by CMIP6 Models. Journal of Climate 33:6471-6489 doi:10.1175/jcli-d-19-0993.1
76. Wang B, LinHo (2002) Rainy Season of the Asian–Pacific Summer Monsoon. Journal of Climate 15:386-398 doi:10.1175/1520-0442(2002)015<0386:Rsotap>2.0.Co;2
77. Wang Y et al. (2008) Millennial- and orbital-scale changes in the East Asian monsoon over the past 224,000 years. Nature 451:1090-1093 doi:10.1038/nature06692
78. Wang Y, He C, Li T (2019) Decadal change in the relationship between East Asian spring circulation and ENSO: Is it modulated by Pacific Decadal Oscillation? Internation Journal of Climatology 39:172-187 doi:https://doi.org/10.1002/joc.5793
79. Wang Y, He C, Li T (2020b) Impact of Global Warming on the Western North Pacific Circulation Anomaly during Developing El Niño. Journal of Climate 33:2333-2349 doi:10.1175/jcli-d-19-0588.1
80. Wang Y, He C, Li T (2020c) Response of the anomalous western North Pacific anticyclone during El Niño mature winter to global warming. Climate Dynamics 54:727-740 doi:10.1007/s00382-019-05024-4
81. Webster PJ, Magaña VO, Palmer TN, Shukla J, Tomas RA, Yanai M, Yasunari T (1998) Monsoons: Processes, predictability, and the prospects for prediction. Journal of Geophysical Research: Oceans 103:14451-14510 doi:10.1029/97jc02719
82. Weldeab S, Lea DW, Schneider RR, Andersen N (2007) 155,000 Years of West African Monsoon and Ocean Thermal Evolution. Science 316:1303-1307 doi:doi:10.1126/science.1140461
83. Xie S-P et al. (2015) Towards predictive understanding of regional climate change. Nature Climate Change 5:921-930 doi:10.1038/nclimate2689
84. Zhang R, Delworth TL (2006) Impact of Atlantic multidecadal oscillations on India/Sahel rainfall and Atlantic hurricanes. Geophysical Research Letters 33 doi:https://doi.org/10.1029/2006GL026267
85. Zhao Y, Harrison SP (2012) Mid-Holocene monsoons: a multi-model analysis of the inter-hemispheric differences in the responses to orbital forcing and ocean feedbacks. Climate Dynamics 39:1457-1487 doi:10.1007/s00382-011-1193-z
86. Zheng W, Wu B, He J, Yu Y (2013) The East Asian Summer Monsoon at mid-Holocene: results from PMIP3 simulations. Climate of the Past 9:453-466 doi:10.5194/cp-9-453-2013
87. Zhou T, Yu R, Li H, Wang B (2008) Ocean Forcing to Changes in Global Monsoon Precipitation over the Recent Half-Century. Journal of Climate 21:3833-3852 doi:10.1175/2008jcli2067.1

88. Zhou W, Xie S-P (2018) A Hierarchy of Idealized Monsoons in an Intermediate GCM. Journal of Climate 31:9021-9036 doi:10.1175/jcli-d-18-0084.1
89. Zuo M, Zhou T, Man W (2019) Hydroclimate Responses over Global Monsoon Regions Following Volcanic Eruptions at Different Latitudes. Journal of Climate 32:4367-4385 doi:10.1175/jcli-d-18-0707.1

Figures

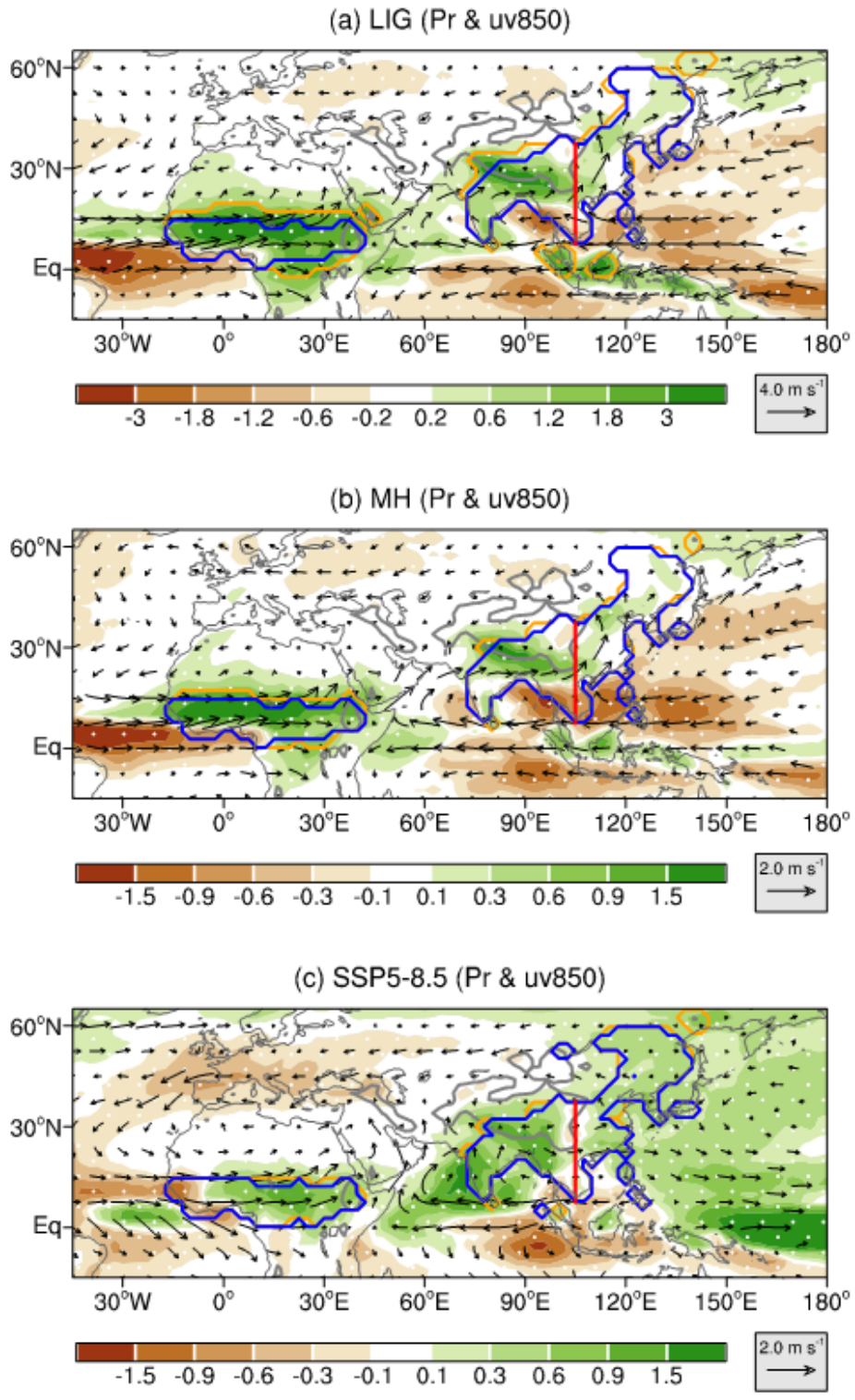

Figure 1

MMM-change of the precipitation (mm day^{-1}) and low-level (850hPa) wind (m s^{-1}) in the (a) Last Interglacial (LIG), (b) Mid-Holocene (MH) and (c) SSP5-8.5 scenario experiment relative to the preindustrial (PIC) experiment. The blue and orange lines denote the land monsoon region in the PIC and the warming epochs respectively. EAM and SAM regions are separated by the red line (105°E). The gray

contour denotes the topography. The dot indicates the change agreed in sigh by at least 70% of the individual model.

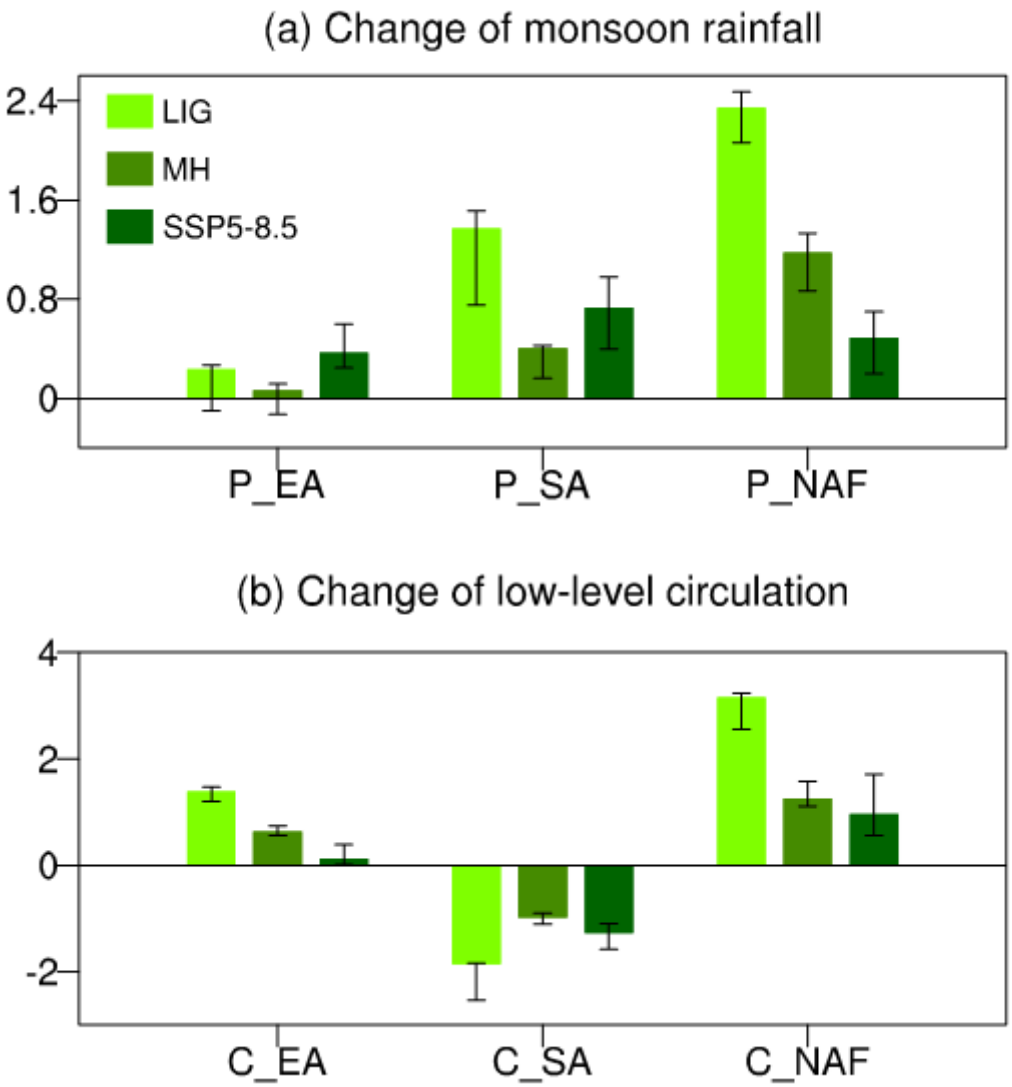

Figure 2

Changes of the (a) monsoon rainfall indices (unit: mm day^{-1}) and (b) low-level monsoon circulation indices (m s^{-1}) in LIG, MH and SSP5-8.5 experiment relative to the PIC experiment. The monsoon rainfall indices are defined as the averaged monsoon rainfall over each monsoon region. The EAM circulation index (C_EA) is defined by the averaged meridional wind (V at 850hPa) over East Asia (20°N-45°N, 110°E-125°E). The SAM circulation index (C_SA) is defined by the westerly over tropical north Indian Ocean (2.5°N-15°N, 55°E-100°E). The NAFM circulation index (C_NAF) is defined as the regional averaged westerly over North Africa (0-12.5°N, 37.5°W-22.5°E). The green bar indicates the MMM, and the thin black bar denotes the range between the 30th and 70th percentiles of the individual models.

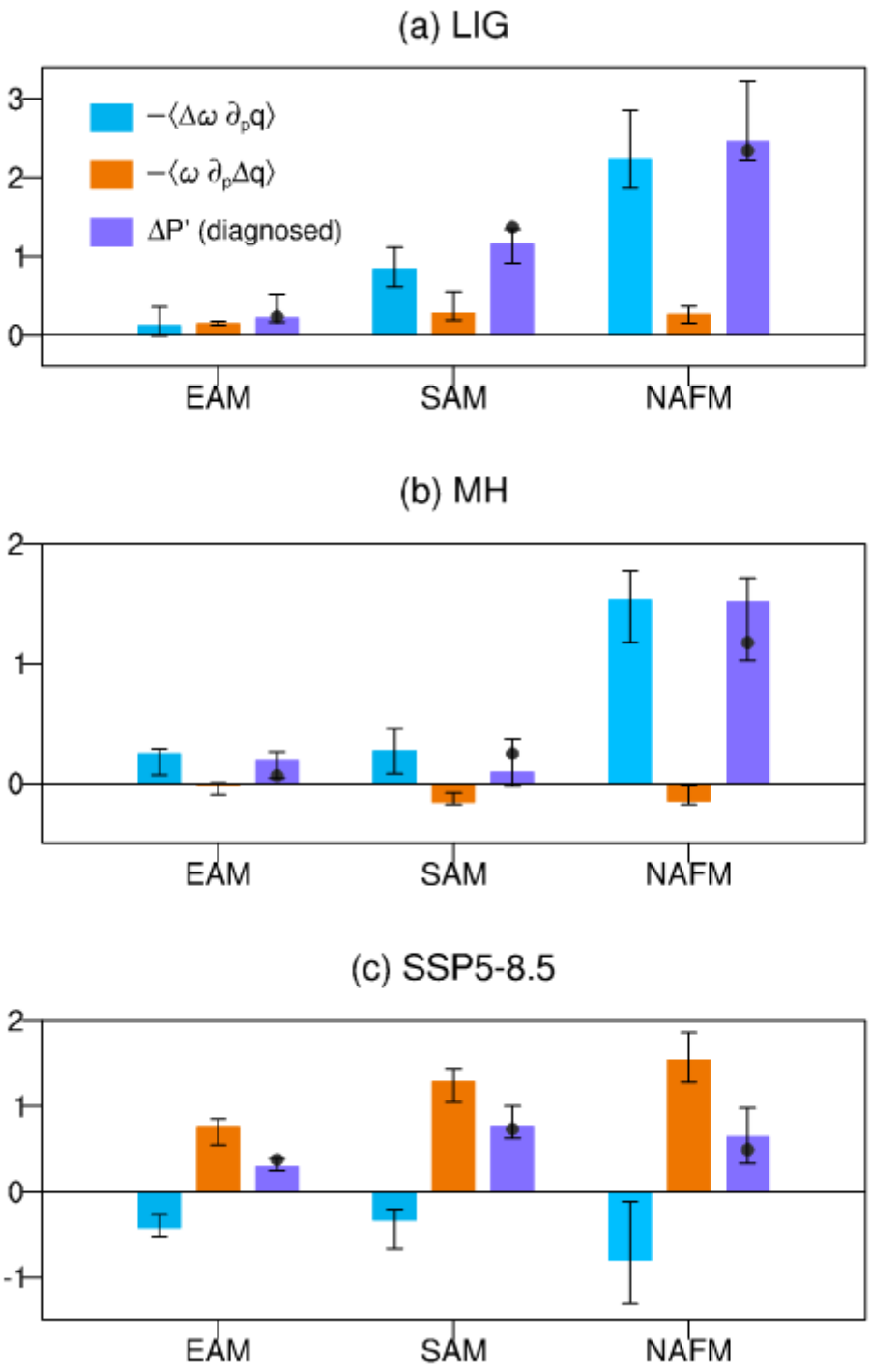

Figure 3

Moisture budget for the change of monsoon rainfall in the (a) LIG, (b) MH and (c) SSP5-8.5 experiment based on the Eq. 3 (unit: mm day^{-1}). The color bar indicates the MMM, and the thin black bar denotes the range between the 30th and 70th percentiles of the individual models. The dots represent the MMM-change of the monsoon rainfall, the magnitude of which is same as the monsoon rainfall indices shown in Fig. 2a.

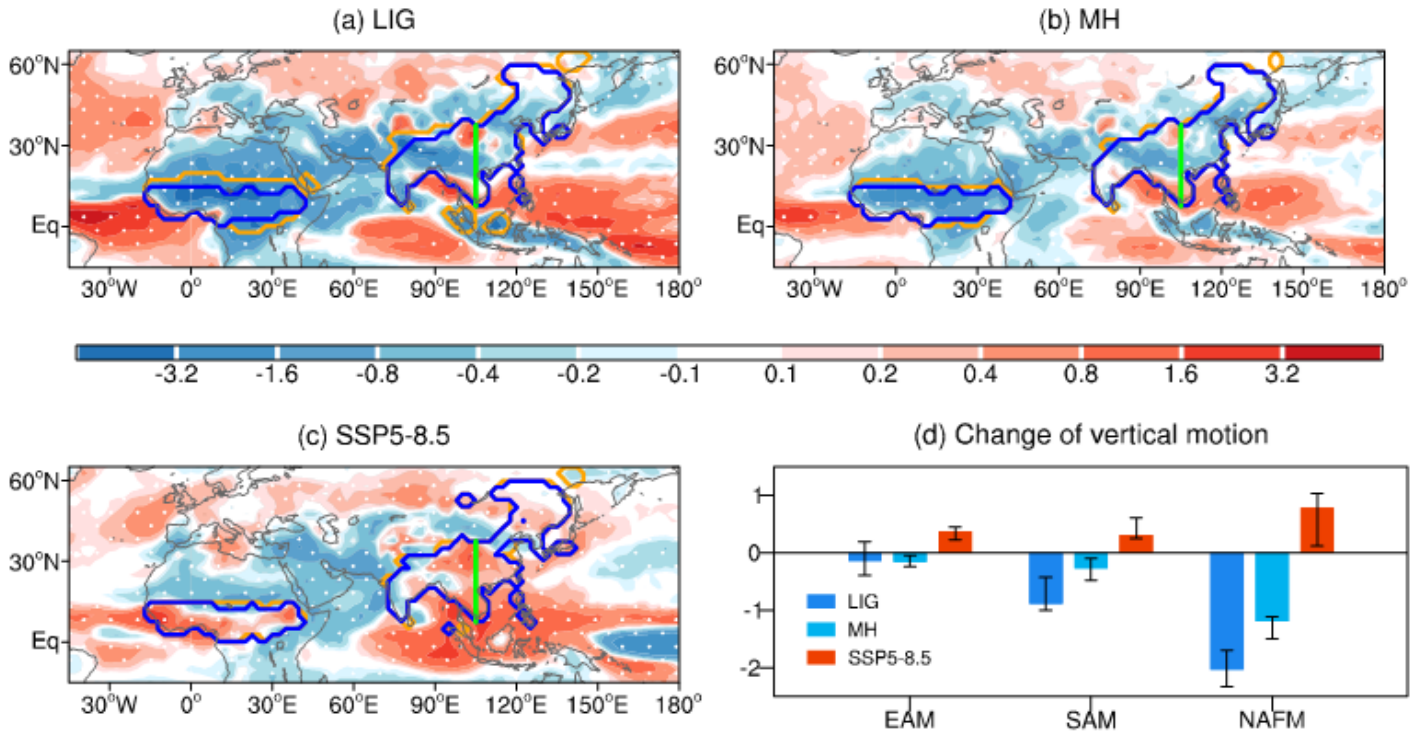

Figure 4

MMM-change of vertical motion (500hPa; unit: 10^{-2} Pa^{-1} s^{-1}) in the (a) LIG, (b) MH and (c) SSP5-8.5 scenario experiment relative to the PIC experiment. Changes agreed in sign by at least 70% of the individual models are stippled. (d) Change of the vertical motion index (VMI; unit: 10^{-2} Pa^{-1} s^{-1}) in different warming epochs, which is defined as the averaged vertical motion at 500hPa within EAM, SAM and NAFM regions. The color bar indicates the MMM, and the thin black bar denotes the range between the 30th and 70th percentiles of the individual models.

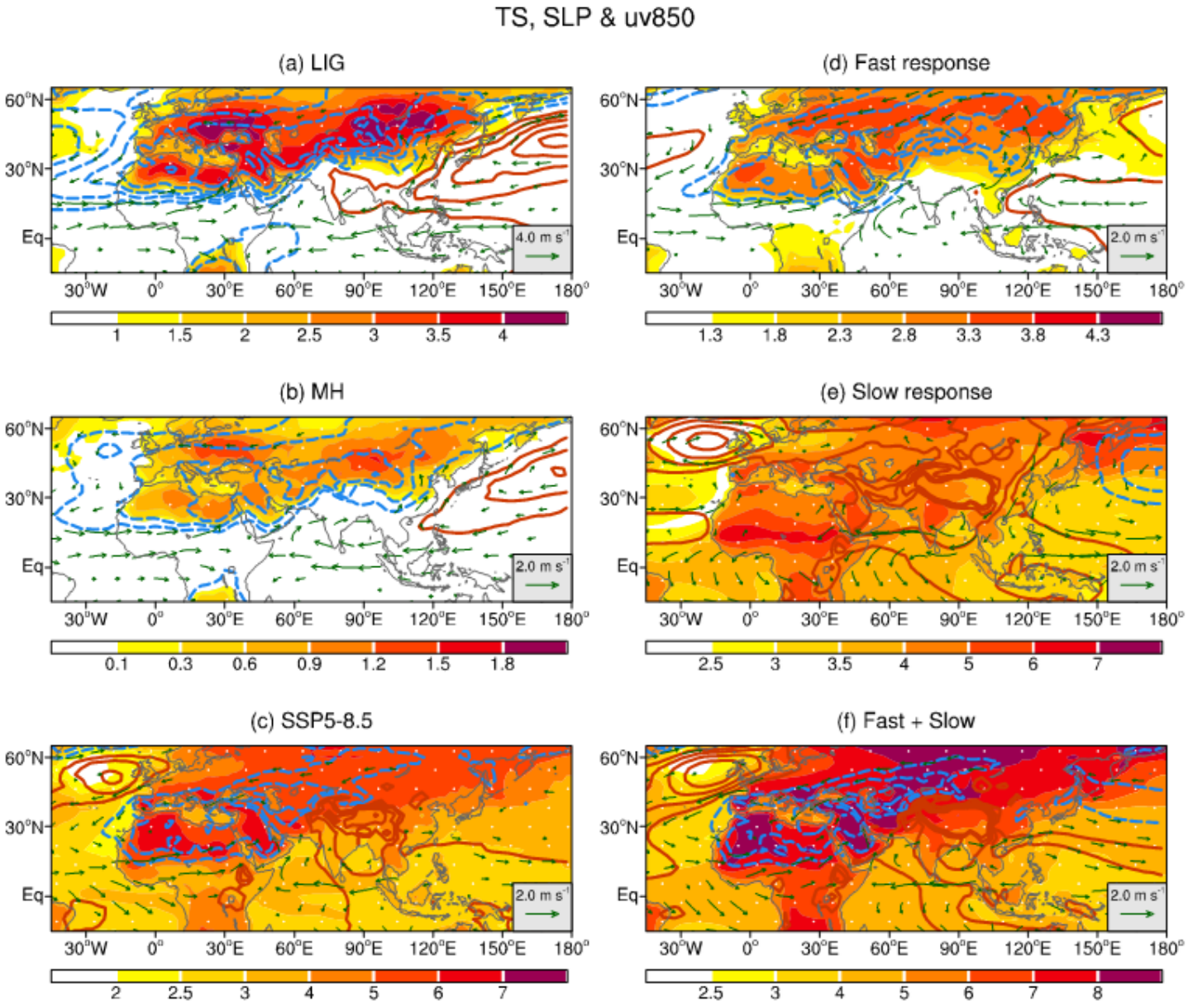

Figure 5

(Left panel) MMM-change of the surface temperature (TS; shading, unit: K), sea level pressure (SLP; contour, unit: Pa) and horizontal wind at 850hPa (vector, unit: m s^{-1}) in the (a) LIG, (b) MH and (c) SSP5-8.5 scenario experiment relative to the PIC experiment. (Right panel) Same as the Left panel, but for the (d) fast response and (e) slow response to the abruptly quadrupling of CO_2 concentration, and (f) their sum. The contours in (a) are from −350Pa to 350Pa with the interval of 70Pa, and the contours in (b)-(f) are from −250Pa to 250Pa with the interval of 50Pa.

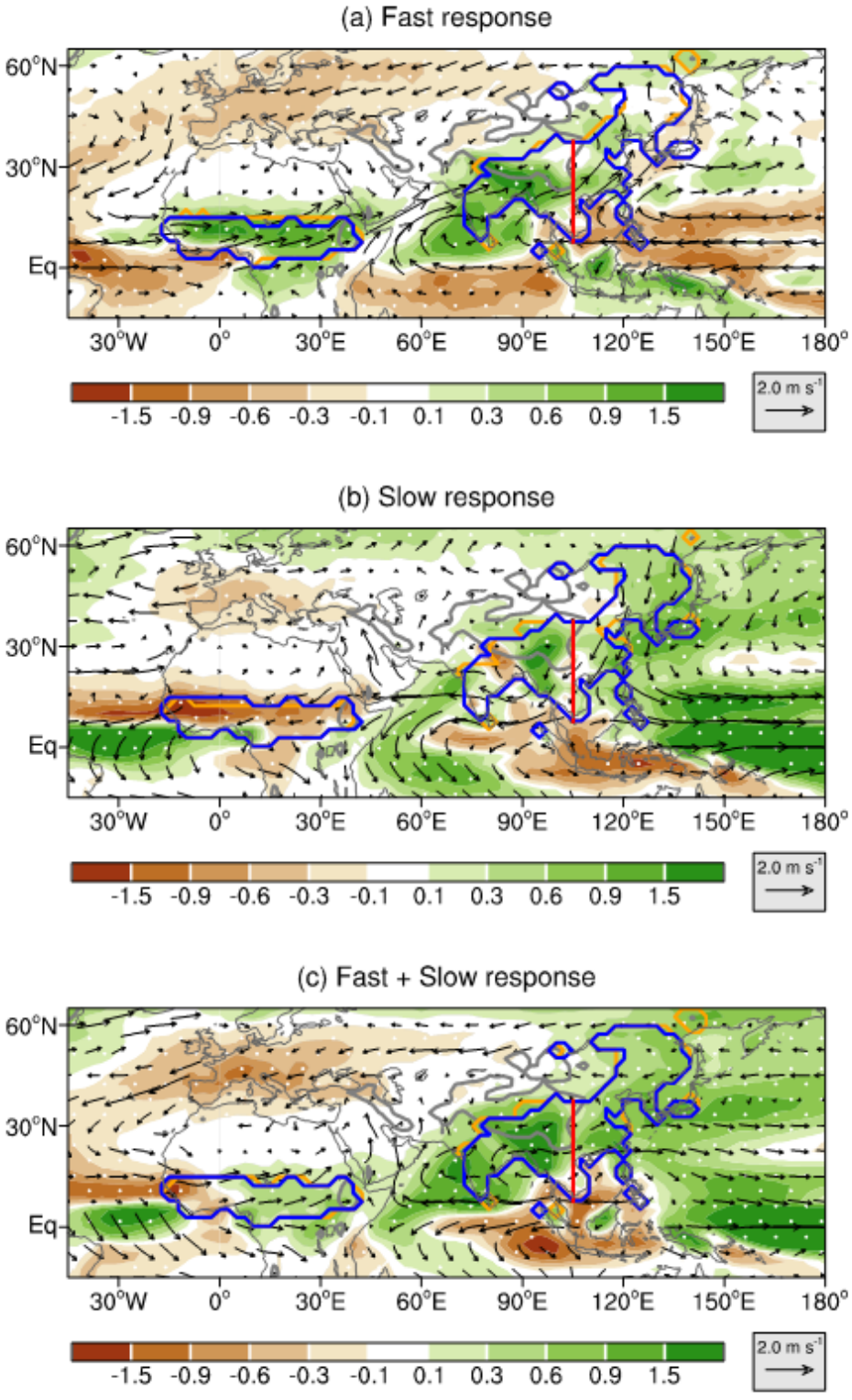

Figure 6

Same as Fig. 1 but for the (a) fast response and (b) slow response to the abruptly quadrupling of CO_2 concentration and (c) their sum.

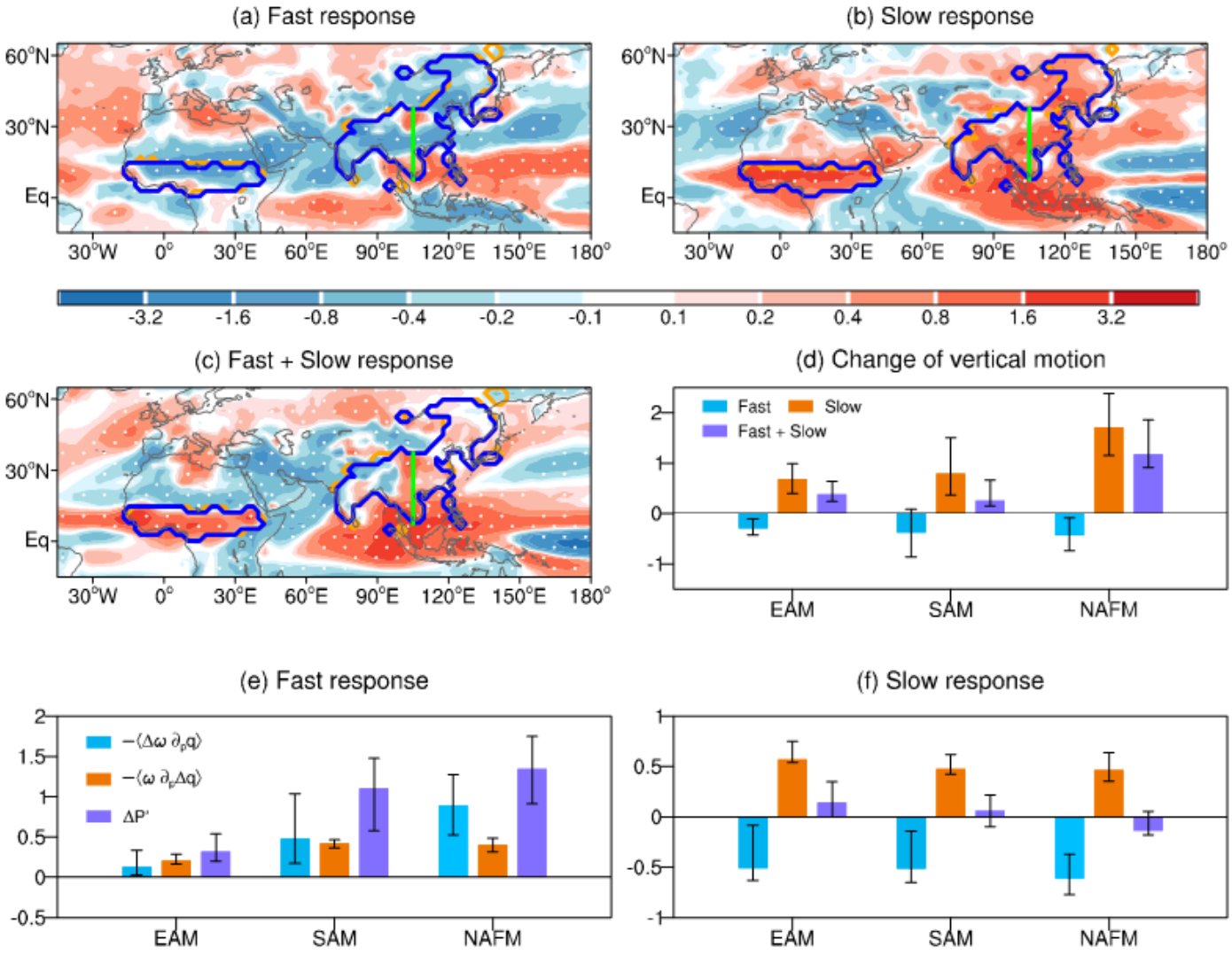

Figure 7

MMM-change of vertical motion (500hPa; unit: 10^{-2} Pa^{-1} s^{-1}) in the (a) fast response and (b) slow response to the abruptly quadrupling of CO_2 concentration and (c) their sum. (d) Change of the vertical motion index (VMI; unit: 10^{-2} Pa^{-1} s^{-1}) in the fast and slow responses and their sum. (e-f) Moisture budget for the monsoon rainfall change in the (e) fast response and (f) slow response based on the Eq. 3. The color bar indicates the MMM, and the thin black bar denotes the range between the 30th and 70th percentiles of the individual models.

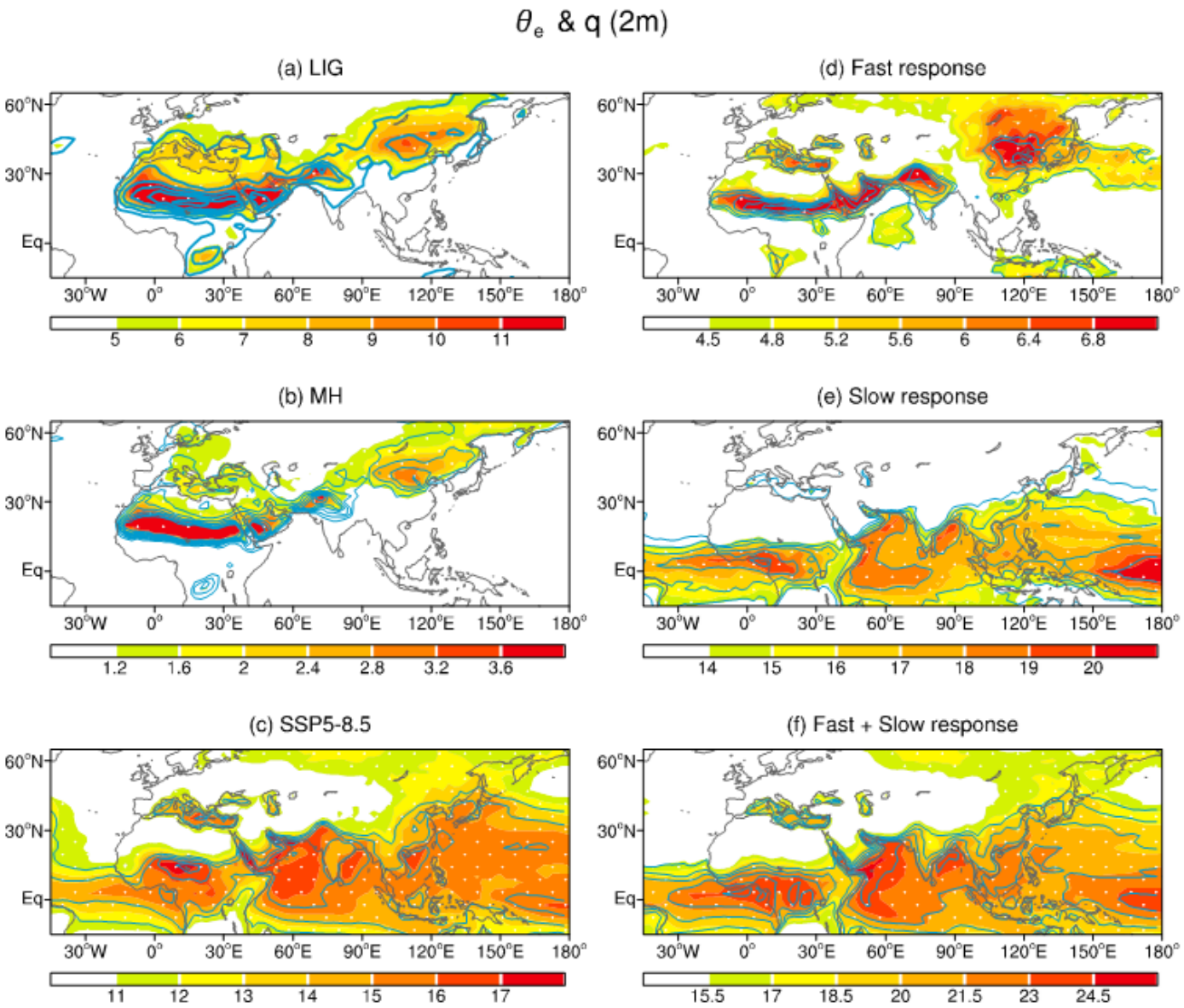

Figure 8

(Left panel) MMM-change of near-surface (2m) equivalent potential temperature (; shading, unit: K) and specific humidity (contour; unit: g kg^{-1}) in the (a) LIG (contour starts from 1 g kg^{-1} with a 1 g kg^{-1} interval), (b) MH (contour starts from 0.2 g kg^{-1} with a 0.4 g kg^{-1} interval) and (c) SSP5-8.5 (contour starts from 3 g kg^{-1} with a 0.5 g kg^{-1} interval) scenario experiment relative to the PIC experiment. (Right panel) Same as the Left panel, but for the (d) fast response (contour starts from 1.2 g kg^{-1} with a 0.2 g kg^{-1} interval) and (e) slow response (contour starts from 3 g kg^{-1} with a 0.5 g kg^{-1} interval) to the abruptly quadrupling of CO_2 concentration and (f) their sum (contour starts from 4 g kg^{-1} with a 0.5 g kg^{-1} interval).

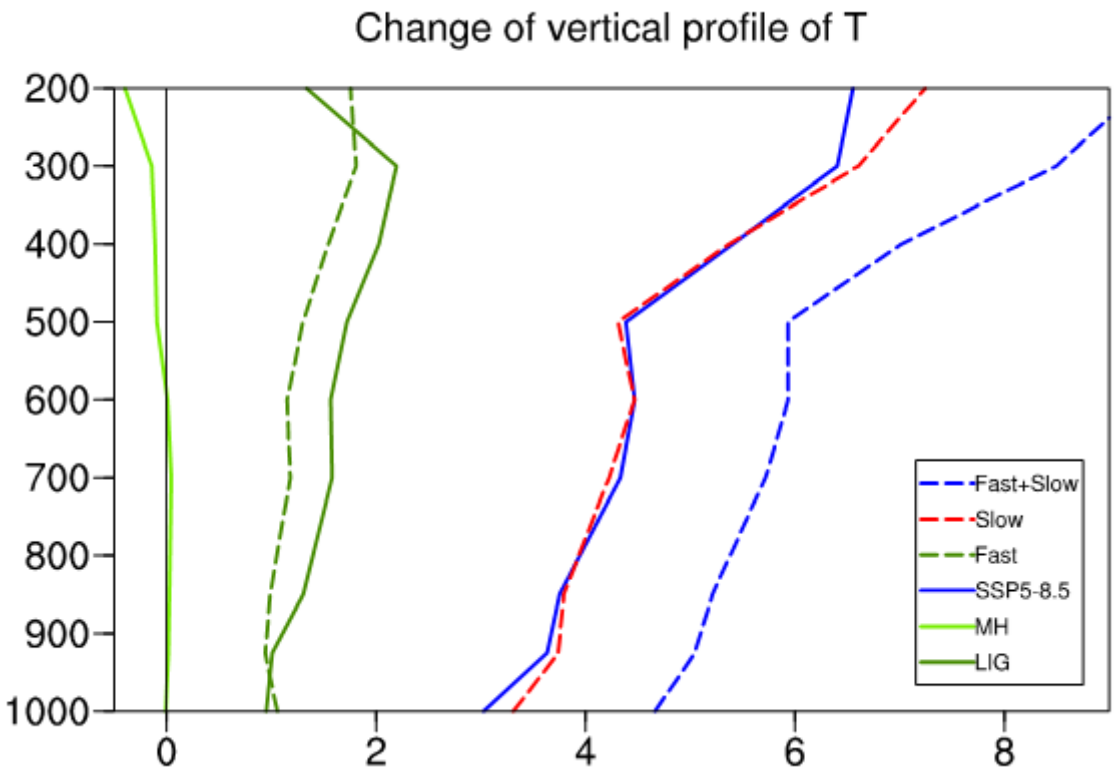

Figure 9

MMM-change of the vertical profile of the tropospheric temperature (unit: K) over the land monsoon region in LIG, MH and SSP5-8.5 scenario experiment relative to the PIC experiment and in the fast response, slow response and their sum.

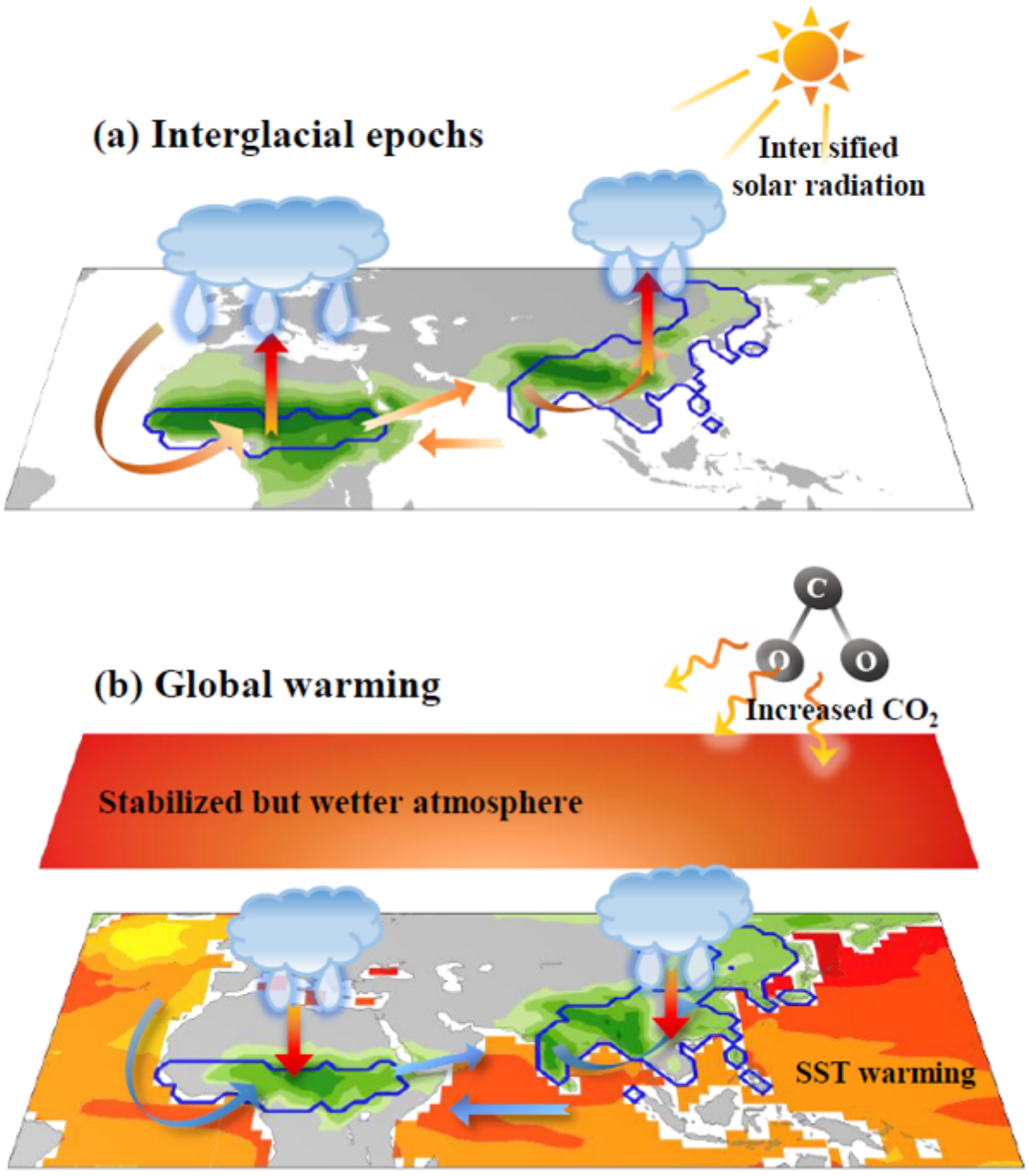

Figure 10

Schematic diagram illustrating the mechanisms for the change of AAM during boreal summer in (a) interglacial epochs and (b) global warming. The blue line indicates the monsoon region, the shading over the ocean and land indicates the SST change and the increased rainfall respectively, and the arrow indicates the monsoon circulation. See the detailed mechanisms in Section 5.

Supplementary Files

This is a list of supplementary files associated with this preprint. Click to download.

- Supplementary20230205.pdf